



RESEARCH ARTICLE

10.1002/2014WR015301

Key Points:

- Probabilistic derivation of flow distribution in seasonally dry climate
- Successfully applied in Nepal, California, and Western Australia
- Disentangles inter- and intra-annual streamflow variations

Correspondence to:

M. F. Müller,
marc.muller@berkeley.edu

Citation:

Müller, M. F., D. N. Dralle, and S. E. Thompson (2014), Analytical model for flow duration curves in seasonally dry climates, *Water Resour. Res.*, 50, 5510–5531, doi:10.1002/2014WR015301.

Received 15 JAN 2014

Accepted 16 JUN 2014

Accepted article online 18 JUN 2014

Published online 7 JUL 2014

Analytical model for flow duration curves in seasonally dry climates

Marc F. Müller¹, David N. Dralle¹, and Sally E. Thompson¹

¹Department of Civil and Environmental Engineering, University of California, Berkeley, California, USA

Abstract Flow duration curves (FDC) display streamflow values against their relative exceedance time. They provide critical information for watershed management by representing the variation in the availability and reliability of surface water to supply ecosystem services and satisfy anthropogenic needs. FDCs are particularly revealing in seasonally dry climates, where surface water supplies are highly variable. While useful, the empirical computation of FDCs is data intensive and challenging in sparsely gauged regions, meaning that there is a need for robust, predictive models to evaluate FDCs with simple parameterization. Here, we derive a process-based analytical expression for FDCs in seasonally dry climates. During the wet season, streamflow is modeled as a stochastic variable driven by rainfall, following the stochastic analytical model of Botter et al. (2007a). During the dry season, streamflow is modeled as a deterministic recession with a stochastic initial condition that accounts for the carryover of catchment storage across seasons. The resulting FDC model is applied to 38 catchments in Nepal, coastal California, and Western Australia, where FDCs are successfully modeled using five physically meaningful parameters with minimal calibration. A Monte Carlo analysis revealed that the model is robust to deviations from its assumptions of Poissonian rainfall, exponentially distributed response times and constant seasonal timing. The approach successfully models period-of-record FDCs and allows interannual and intra-annual sources of variations in dry season streamflow to be separated. The resulting median annual FDCs and confidence intervals allow the simulation of the consequences of interannual flow variations for infrastructure projects. We present an example using run-of-river hydropower in Nepal as a case study.

1. Introduction

In 2010, about 30% of the world's population lived in areas that experience Mediterranean, Monsoonal, or Savanna climates [CIESIN, 2012], which are characterized by strong seasonality in rainfall. In these climates, annual precipitation is concentrated within one or two wet seasons, followed by extended dry periods. The availability of surface water for ecosystem services (e.g., ecology, domestic supply, irrigation, power generation, or sediment transport) during the dry season is strongly dependent on the precipitation volume during the previous wet season and its subsequent discharge from watersheds [Jothityangkoon and Sivapalan, 2001; Samuel et al., 2008; Andermann et al., 2012]. For instance, in the central Himalayas, up to 80% of the annual rainfall occurs during the 3 month long Indian Summer Monsoon (ISM) season. Transient storage of water in fractured bedrock during the rising ISM, and its post-ISM release form the dominant source of dry season streamflow [Andermann et al., 2012], dwarfing the effect of other drivers like evapotranspiration and snow/glacial melt. Because the timing and intensity of precipitation in seasonally dry climates exhibits large interannual variation [Fatichi et al., 2012] that will likely be amplified by climate change [e.g., Dominguez et al., 2012; García-Ruiz et al., 2011], both wet season input and dry season water availability are also strongly variable.

In this context, the equitable allocation of seasonally scarce water resources and the design of water-dependent infrastructure are strongly dependent on the reliable prediction of surface water availability and reliability. A key tool used to represent this information is the flow duration curve (FDC): a graphical representation of the probability that a specific magnitude of streamflow is equaled or exceeded [Castellarin et al., 2013]. Mathematically, the FDC can be computed as the complement of the cumulative density function (CDF) of daily streamflow. A FDC provides a frequency-domain representation of the daily runoff time series, providing a compact signature of streamflow variability, and its underlying drivers. FDCs are commonly used to estimate water availability for hydropower [e.g., Basso and Botter, 2012], water supply and irrigation [e.g., Chow, 1964], waste load allocation [e.g., Searcy, 1959], reservoir management [e.g., Alaouze,

1989], and environmental health [e.g., *Acreman and Dunbar*, 1999]. A comprehensive review of practical FDC applications is presented in *Vogel and Fennessey* [1995].

Despite the utility of FDCs, they are also data intensive, requiring long-term, on-site daily runoff measurements for their computation [*Vogel and Fennessey*, 1994]. In many parts of the world such data are only sparsely available. The development of techniques to regionalize FDCs to ungauged basins therefore remains an active area of research, especially in arid areas, where the performance of existing methods decreases significantly [*Castellarin et al.*, 2013]. Regionalization commonly employs data-intensive statistical approaches, and the calibration of these methods also relies on the availability of long streamflow time series from a large number of representative and well-characterized catchments [e.g., *Cheng et al.*, 2012; *Coopersmith et al.*, 2012]. Thus, traditional regionalization of FDCs remains challenging in truly data-scarce regions. Furthermore, statistical approaches are not able to distinguish the effects of nonstationary climates from those of changing landscape properties, making their application for future flow predictions challenging.

Simple but process-based models of the FDC have the potential to circumvent both of these issues [e.g., *Botter et al.*, 2007a; *Ye et al.*, 2012]. Such models can be developed by extending existing analytical solutions for the probability density function (PDF) of streamflow. In particular *Botter et al.* [2007a] analyzed the effect of rainfall forcing on soil moisture and water table recharge. Under the assumption that rainfall occurs as a Poisson Process and that the response time distribution in the water table is exponential, base flow contribution to streamflow follows a gamma distribution. The resulting streamflow PDF depends on a limited number of physically meaningful parameters related to the stochastic structure of rainfall, and to the soil, vegetation, and geomorphologic properties of the catchment. The inherently process-based nature of the approach reduces calibration requirements, allows the effects of changes in climate or the landscape to be independently modeled, and in principle could be driven by remote-sensing observations of rainfall and climate, even where ground-based measurements are sparse [*Müller and Thompson*, 2013].

This probabilistic approach has been successfully used to model streamflow PDFs in catchments in the United States, Italy, and Switzerland [*Botter et al.*, 2007b; *Ceola et al.*, 2010; *Schaefli et al.*, 2013; *Botter et al.*, 2013]. Two issues, however, need to be addressed before extending the approach to seasonally dry climates. The first issue is general: if these approaches are to be pragmatically used for flow forecasting in multiple basins, then it is likely that the rainfall distribution in at least some of these basins will not be well described by a Poisson process [*Katz and Parlange*, 1996; *Müller and Thompson*, 2013]. Similarly, deviations from an exponential travel time distribution within the water table are likely in some basins. Although streamflow PDFs for basins with some nonexponential travel time distributions can be determined analytically [*Botter et al.*, 2009], they are more complex and less analytically tractable than the gamma distribution form. It is therefore valuable to determine how robust the model predictions to deviations from idealized rainfall and catchment properties, and when the simplest PDF description remains valid. The second issue recognizes that previous PDF forecasting with these techniques addressed only seasonal subsets of streamflow time series, where there is an interplay between stochastic water inputs through rainfall, and recessions, through which the excess water is released as streamflow. Yet in seasonally dry climates, where the flow regime during an entire season can be driven by the release of water stored in the catchment prior to the considered season (e.g., *Andermann et al.* [2012] in Nepal), the simple analytical model fails because the system does not experience a stochastic Poisson forcing.

In this paper, we extend *Botter et al.* [2007a] to link wet and dry season flow generation mechanism and predict annual streamflow distributions in seasonally dry climates. The research is aimed at investigating the following two hypotheses:

H1: Within identifiable limits, the streamflow distribution model described in [*Botter et al.*, 2007a] is robust to deviations from Poissonian precipitation inputs and exponential travel time distributions in the water table.

H2: Streamflow probability distributions during the dry season can be constructed from a deterministic recession relationship with a stochastic initial condition that captures interannual variability in wet season characteristics.

We derive analytical expressions for FDCs for seasonally dry watersheds from the superposition of wet season (Hypothesis 1) and dry season (Hypothesis 2) distributions, and evaluate these hypotheses in three different locations with markedly different geologic contexts and distinct climatologies (Figure 1): (a) Nepalese Himalayas (topographically complex, deep and shallow soils, Monsoonal), (b) Coastal California

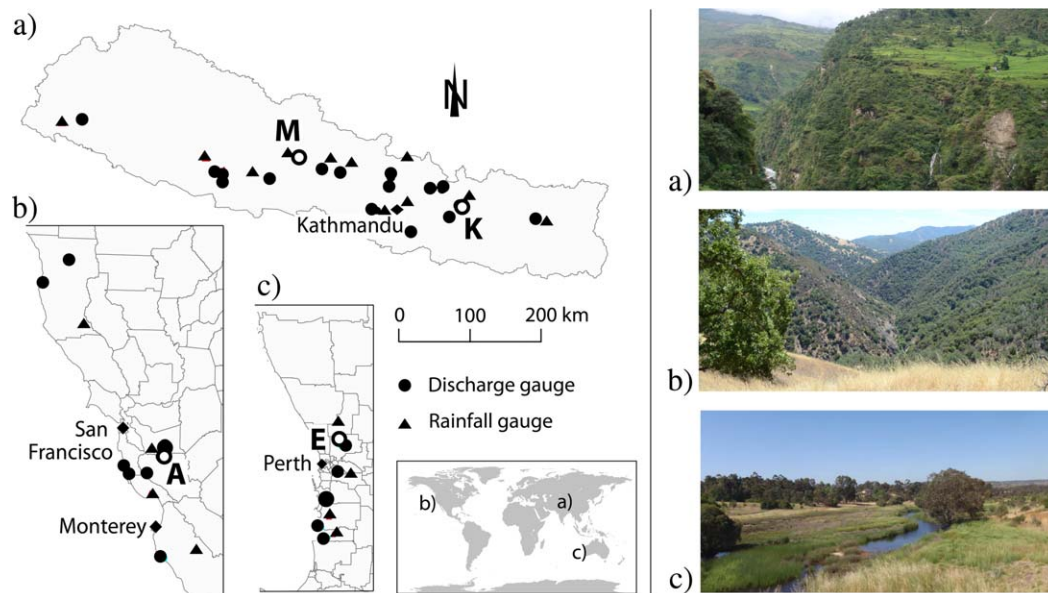


Figure 1. Respective locations of the 17, 8 and 6 Discharge gauges and corresponding rainfall gauges in (a) Nepal, (b) California, and (c) Western Australia. Parameters have been estimated using rainfall on the Modi Kohla (M) and Khimti Kohla (K) catchments in Nepal and Ellenbrook (E) in Western Australia because of their small surface area and proximity to a rain gauge. Photo credits: (a) Marc Müller, (b) Gopal Penny, (c) Artemis Kitsios.

(topographically complex, shallow soils, Mediterranean), and (c) Western Australia (flat, deep soils, Mediterranean). We illustrate the practical relevance of the derived analytical method by forecasting the electricity production of two run-of-river hydropower plants in Nepal.

2. Methods

2.1. Theory

This section describes the derivation of an analytical expression for FDCs in seasonally dry climates. Unless otherwise specified, upper case characters denote random variables and corresponding lower case characters denote realizations of these random variables. The PDF and CDF of a random variable X taken at x are, respectively, written $p_X(x)$ and $P_X(x)$. Complete, upper incomplete and lower incomplete gamma functions are noted $\Gamma(\cdot)$, $\Gamma_U(\cdot, \cdot)$ and $\Gamma_L(\cdot, \cdot)$, respectively.

The derivation is based on the following key assumptions. Several of these assumptions are necessary for the wet season flow model and reflect those made by Botter *et al.* [2007a] in its original derivation. The remaining assumptions pertain to the current extension to seasonally dry systems:

1. The watersheds are small enough so that rainfall, soil, and vegetation properties can be treated as being spatially homogenous [Botter *et al.*, 2007a].
2. The contribution of glacier or snowmelt is negligible, so that rainfall is the dominant stochastic driver of streamflow [Botter *et al.*, 2007a]. This assumption allows the effects of stochasticity in temperature and solar irradiation to be neglected as drivers of flow variability. While the model does not apply to watersheds, where glacial or snowmelt discharge is dominant, it can be adapted for snow-fed basins without seasonal snowpack accumulation [Schaefli *et al.*, 2013].
3. There are two distinct precipitation seasons (wet and dry) characterized by a statistically significant difference in mean seasonal streamflow. The duration of the seasons is assumed to be near-constant from year to year, so that the effects of interannual variations in the timing of the seasons have minimal impact on the stochasticity of flow.
4. During the rainy season, rainfall is assumed to follow a marked Poisson process with exponentially distributed rainfall intensities. When infiltrated rainfall causes soil moisture to exceed the field capacity of the vadose zone, excess water recharges the water table and is available to generate runoff [Botter *et al.*, 2007a].

5. The response time distribution during the wet season is treated as exponential [Botter et al., 2007a].
6. During the dry season, the (minimal) rainfall is assumed to be completely consumed by evapotranspiration in the vadose zone. Thus, this simple model assumes that there is no water transfer between the vadose zone and the water table in the dry season, and only water stored during the previous rainy season drains and feeds the base flow of the stream.

We assess the sensitivity of the model to violations in three key dynamic assumptions—binary seasonality, the Poissonian character of rainfall in the wet season, and the constant length of each season—through numerical simulations and via case study on watersheds in Nepal, Coastal California, and Western Australia.

2.1.1. Steady State Rainy-Season Streamflow Distribution

Under these assumptions, the vadose zone censors the frequency of rainfall. If the incoming rainfall is a marked Poisson process, wet-season runoff increments also follow a marked Poisson process [Botter et al., 2007a]. The censored runoff frequency λ is related to rainfall frequency λ_p by [Rodríguez Iturbe and Porporato, 2004; Botter et al., 2007a]:

$$\lambda = \eta \frac{\exp(-\gamma) \gamma^{\frac{\lambda_p}{\eta}}}{\Gamma_L(\lambda_p/\eta, \gamma)}, \tag{1}$$

where $\eta = ET / (nZ_r(s_1 - s_w))$ is the maximum evapotranspiration rate normalized by the root zone storage capacity, and $\gamma = \gamma_p nZ_r(s_1 - s_w)$ is the ratio between the soil storage capacity and the mean rainfall depth $1/\gamma_p$. Z_r , n , s_1 and s_w are parameters, respectively, representing the depth, porosity, field capacity, and wilting point of the root zone and are defined by vegetation and soil type.

Assuming an exponential distribution of travel time in the water table, the steady state distribution of rainy-season streamflow Q_w follows a gamma distribution [Botter et al., 2007a]:

$$p_{Q_w}(q_w) = \frac{\gamma_Q^m}{\Gamma(m)} q_w^{(m-1)} \exp(-\gamma_Q q_w), \tag{2}$$

$$P_{Q_w}(q_w) = \frac{\Gamma_L(m, \gamma_Q q_w)}{\Gamma(m)} \tag{3}$$

with $Q \in \mathbb{R}_{\geq 0}$. The parameter $m = \lambda/k$ describes the ratio between the mean response time ($1/k$) and mean interarrival time ($1/\lambda$) of recharge events to the aquifer. The inverse of the mean recharge volume is given by

$$\gamma_Q = \frac{\gamma_p}{Ak}, \tag{4}$$

with γ_p the mean inverse rainfall intensity and A the contributing area of the watershed. Equations (2) and (3) assume small (i.e., smaller than rainfall spatial correlation lengthscale) and homogenous basins, with flow and rainfall measured on time scales larger than the characteristic duration of single rainfall events (e.g., daily streamflow). It does not account for lateral subsurface flow in the vadose zone, losses to deep percolation or overland flow.

2.1.2. Peak Flow Distribution of the Last Rainy Season Storm

Typically, the time scale of the exponential correlation function of the Poisson rainfall process is short enough that streamflow rapidly reaches a steady state following the onset of the wet season. This steady state streamflow can thus be modeled by a random variable Q_w with a PDF given by equation (2). The dry season recession begins at the realization of Q_w on the last day of the wet season (i.e., at $t = T_w$), which is defined here as occurring at the peak of the last storm of the wet season. The flow Q_0 that represents the initial condition at the beginning of the dry season is thus the sum of two stochastic processes: the flow Q_w discharged before the last wet season storm and the flow increment Δ generated by the precipitation during that storm:

$$Q_0 = Q_w + \Delta$$

With the assumptions above [Botter et al., 2007a], flow increments are independent and exponentially distributed with mean $1/\gamma_Q$.

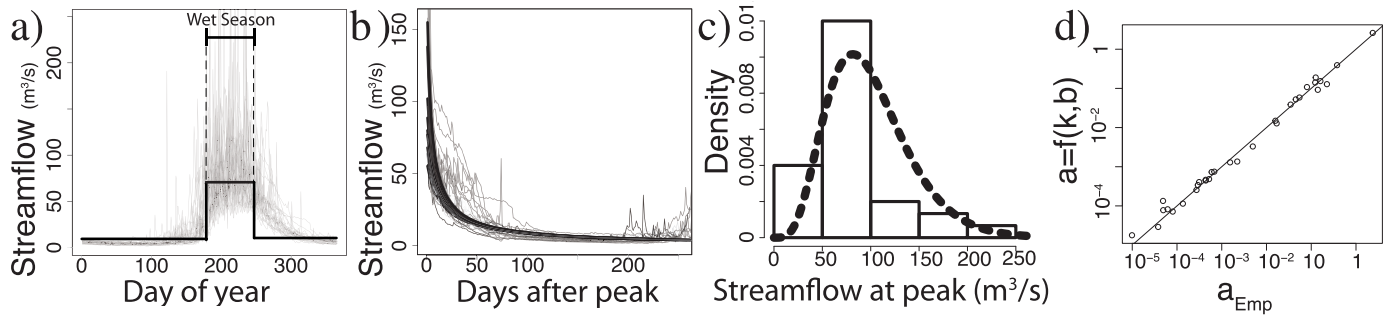


Figure 2. (a) Estimation of the seasonality parameter at Khimti Kohla. The first vertical segment of the step function represents the median starting day of the wet-season flow regime. The length of the following segment represents the median time until the last wet-season discharge peak. (b) Seasonal recession estimation at Khimti Kohla. Dark lines are fitted recessions for $a = 0.00089$ and $b = 2.09$ given the observed initial streamflow. (c) Empirical histogram of the Khimti Kohla discharge at the end of the wet season for $N = 30$ years. The histogram is overlaid by the analytical PDF computed from equation (6). (d) Scatterplot of empirical a parameters estimated on the 31 considered catchments against corresponding values obtained from equation (23). The solid line represents $a_{Emp} = a(k, b)$, $R^2 = 0.98$.

$$p_{\Delta}(q_w) = \gamma_Q \exp(-\gamma_Q q_w) \tag{5}$$

with $q \in \mathbb{R}_{\geq 0}$. Because the distribution of the sum of two independent random variables is given by the convolution of the distributions of the individual random variables, the PDF and CDF of the streamflow at the end of the wet season can be expressed by convolving p_{Δ} and p_{Q_w} .

$$\begin{aligned} p_{Q_0}(q_0) &= \int_0^{q_0} p_{Q_w}(q_w) p_{\Delta}(q_0 - q_w) dq_w \\ &= \frac{\gamma_Q^{1+m}}{\Gamma(m+1)} \exp(-\gamma_Q q_0) q_0^m \end{aligned} \tag{6}$$

$$P_{Q_0}(q_0) = \frac{\Gamma_L(1+m, \gamma_Q q_0)}{\Gamma(m+1)}, \tag{7}$$

The integration in equation (6) is bounded by q_0 because the domain of $p_{\Delta}(q_w)$ (equation (5)) is nonnegative. Q_0 follows a gamma distribution with rate γ_Q identical to the rate of Q_w and Δ and with a shape parameter $m + 1$. The expectation of Q_0 can be expressed as:

$$E[Q_0] = \frac{m+1}{\gamma_Q} \tag{8}$$

Q_0 is thus an annual stochastic variable representing the interannual variability of the intensity of the rainy season (Figure 2c).

2.1.3. Modeling Recession Relations

Following *Andermann et al.* [2012], we hypothesize that dry season streamflow is driven by the release of water stored in the water table during the previous rainy season. We neglect the contribution of snow and glacial melt and of dry season precipitation. During the rainy season, frequent recharge events minimize variations of the water table level. Under these circumstances, the Boussinesq equation, which governs water table discharge to the channel, is well approximated by its linearized solution, which is characterized by an exponential travel time distribution [*Brutsaert and Nieber, 1977*] and an exponential recession of base flow in the absence of recharge.

$$Q_w(t) = q_{wo} e^{-kt} \tag{9}$$

where parameter k is the linear recession constant and q_{wo} the peak flow at the beginning of the recession.

Once frequent recharge ceases during the dry season, however, the water table undergoes a large transient drawdown, corresponding to nonlinear discharge behavior and a power-law response time distribution [Brutsaert and Nieber, 1977]:

$$\frac{dQ}{dt} = -aQ^b \tag{10}$$

Here parameters a and b are assumed stationary and are related to aquifer characteristics (depth, surface area, hydraulic conductivity, porosity, and drainage density), and to the boundary and initial conditions for the water table. Integrating equation (10) provides the temporal evolution of the dry-season flow Q_d given an initial discharge q_0 [Brutsaert and Nieber, 1977]

$$Q_d(t) = (q_0^r - art)^{\frac{1}{r}} \tag{11}$$

where $r = 1 - b$. Equation (11) provides a reasonable description of observed seasonal recessions, as qualitatively shown in Figure 2b.

2.1.4. Dry-Season Streamflow Distribution

Inverting equation (11) allows the time t^* needed for the recession flow to reach the condition $Q_d(t) \leq Q$ to be computed. Then, knowing that $Q_d(t)$ is decreasing, streamflow always meets the condition $Q_d \leq Q$ during the period between t^* and the end of the dry season. This allows the CDF of Q_d conditional on the initial flow Q_0 to be found as (see Appendix A):

$$P_{Q_d|Q_0=q_0}(q_d, q_0) = P\{Q_d \leq q_d | Q_0 = q_0\} = \frac{|\{t \in [0, T_d] | Q_d(t) \leq q_d\}|}{T_d} = \begin{cases} 1, & \text{if } q_d > q_0 \\ 0, & \text{if } q_d < (K - arT_d)^{\frac{1}{r}} \\ 1 - \frac{1}{T_d} \frac{q_0^r - q_d^r}{ar}, & \text{otherwise} \end{cases} \tag{12}$$

where parameter T_d is the duration of the dry season and where $K = q_0^r$ if $r > 0$ and $K = 0$ if $r < 0$ (implying that $0 < b < 1$).

Knowing the distribution of Q_0 (equation (6)), we obtain the unconditional cumulative density function of dry season flow by applying the law of total probabilities [Sornette, 2004]:

$$P_{Q_d}(q_d) = \int_{Q_0} P_{Q_d|Q_0}(q_d, q_0) p_{Q_0}(q_0) dq_0 = \begin{cases} 1 + \frac{q_d^r \Gamma_1 - \gamma_Q^{-r} \Gamma_2}{arT_d \Gamma(m+1)}, & \text{if } q_d > -(arT_d)^{\frac{1}{r}} \text{ and } r < 0 \\ 1 + \frac{q_d^r \Gamma_1 - \gamma_Q^{-r} \Gamma_2}{arT_d \Gamma(m+1)} + \frac{\gamma_Q^{-r} \Gamma_4 + (q_d^r - arT_d) \Gamma_3}{arT_d \Gamma(m+1)}, & \text{otherwise} \end{cases} \tag{13}$$

with

$$\begin{aligned} \Gamma_1 &= \Gamma_U(m+1, \gamma_Q q_d) \\ \Gamma_2 &= \Gamma_U(r+m+1, \gamma_Q q_d) \\ \Gamma_3 &= \Gamma_U\left(m+1, \gamma_Q (q'_d + arT_d)^{\frac{1}{r}}\right) \\ \Gamma_4 &= \Gamma_U\left(r+m+1, \gamma_Q (q'_d + arT_d)^{\frac{1}{r}}\right) \end{aligned}$$

Full derivations of equations (12) and (13) are provided in Appendix A.

2.1.5. Period-of-Record Flow Duration Curve

Thanks to the memoryless property of the exponentially distributed runoff increments $\Delta^+ Q_{storm}$, the flow Q_0 representing the initial condition at the beginning of the dry season can reasonably be assumed independent from wet-season daily streamflow Q_w . Daily discharge during the wet and daily discharge during the dry season are therefore two independent random variables and the CDF of streamflow (unconditional on the season) can be expressed as a weighted average of the underlying seasonal CDFs (equations (3) and (13)) [Botter et al., 2008]:

$$P_Q(q) = \left(1 - \frac{T_d}{365}\right) \cdot P_{Q_w}(q) + \frac{T_d}{365} \cdot P_{Q_d}(q) \tag{14}$$

The period-of-record flow duration curve (PoRFDC) is computed by inserting the unconditional CDFs of wet and dry season streamflow (equations (3) and (13)) and plotting the streamflow quantiles q against $1 - P_Q(q)$, the complement of the assembled streamflow CDF.

2.1.6. Annual Flow Duration Curves

While the PoRFDC lumps the intra and interannual character of streamflow variations, variability on these two time scales can be separated using annual flow duration curves (AFDC). Empirical ADFCs are constructed for each year using the streamflow records for that year only. The quantile-by-quantile median of the exceedance probabilities from all available ADFCs and their related confidence intervals describe the flow regime of a typical (though hypothetical) year and its interannual variation [Vogel and Fennessey, 1994]. Both of these can be quite different from the PoRFDC. The information provided by ADFCs is of particular relevance in water resource management applications, where costs and benefits are calculated on a yearly basis, and where the high degree of interannual variability characteristic of seasonally dry climates has direct implication for infrastructure design.

In the proposed model, dry season base flow is driven by an annual stochastic process—the streamflow Q_0 generated following the last wet season storm, and a deterministic intra-annual recession. These features mean that intra and interannual streamflow variation can be readily disentangled. During the wet season, we model daily streamflow Q_w as the product of two independent random variables: an annual stochastic index flow $Q_{AF,w}$ and a dimensionless daily streamflow $Q'_{w,t}$. This stochastic index flow approach has been successfully applied to predict both PoRFDCs and ADFCs in ungauged basins [Castellarin et al., 2007] and was recently adapted for intermittent streams [Rianna et al., 2013]. Here, we consider mean runoff as the stochastic index flow for the wet season:

$$Q_{AF,w} = \frac{1}{T_w} \sum_{t=1}^{T_w} Q_{w,t}, \tag{15}$$

where $T_w = 365 - T_d$ is the (assumed constant) duration of the wet season. Because all daily realizations $Q_{w,t}$ of wet season base flow follow an identical gamma distribution, the CDF of $Q_{AF,w}$ is a linear transformation of the T_w -fold convolution of the CDF of Q_w given in equation (3):

$$P_{Q_{AF,w}}(q_{AF,w}) = P_{Q_w}^{T_w*}(T_w \cdot q_{AF}) = \frac{\Gamma_L(T_w \cdot m, T_w \cdot \gamma_Q q_{AF,w})}{\Gamma(T_w \cdot m)}, \quad (16)$$

where $P_{Q_w}^{T_w*}$ denotes the T_w -fold convolution of the CDF of Q_w . The dimensionless daily streamflow Q'_w during the wet season is obtained by dividing Q_w by its expectation. Its CDF can be expressed as:

$$P_{Q'_w}(q'_w) = P_{Q_w}(\mu_{Q_w} \cdot q'_w) = \frac{\Gamma_L(m, m \cdot q'_w)}{\Gamma(m)}, \quad (17)$$

where $\mu_{Q_w} = \frac{m}{\gamma_Q}$ is the expectation of Q_w .

The CDF of annual quantile n (e.g., $n \in \{0.5, 0.05, 0.95\}$) provides the median AFDC and the bounds of its 90% confidence interval) can be expressed as:

$$P_{Q_{In}}(q) = \left[1 - \frac{T_d}{365}\right] \cdot P_{Q'_w}\left(\frac{q}{Q_{AF,w}^{(n)}}\right) + \frac{T_d}{365} \cdot P_{Q_d|Q_0=q_0}(q, Q_0^{(n)}), \quad (18)$$

where $Q_{AF,w}^{(n)}$ and $Q_0^{(n)}$ are the n -quantile realizations of $Q_{AF,w}$ and Q_0 , that is the inverse function (taken at quantile n) of the CDFs of equations (16) and (7). $P_{Q'_w}$ and $P_{Q_d|Q_0=q_0}$ are the CDFs representing the intra-annual streamflow variations in the wet (equation (17)) and dry (equation (12)) seasons. Since the function $Q_d(t)$ is monotonic in Q_0 (equation (11)), larger realizations of Q_0 lead to larger values of $Q(t)$ everywhere. As a result $Q_0^{(n)}$, the n -quantile realization of Q_0 , corresponds to the n -quantile realization of $Q_d(t)$ for all t . Therefore, inserting the resulting $Q_0^{(n)}$ into the conditional dry-season CDF (equation (12)) allows analytical expressions for the median AFDC and the considered confidence interval to be derived during the dry season despite Q_0 and Q_d being correlated.

2.2. Parameter Estimation

The derived model has six parameters ($T_d, \lambda, \gamma_Q, a, b, k$) related to rainfall and catchment properties. These parameters can be estimated from streamflow or rainfall time series as described below. Summary statistics of the parameters estimated for the case studies are given in Table 1.

2.2.1. Rainfall Parameters

The frequency λ and mean intensity $1/\gamma_Q$ of wet-season runoff events and the duration T_d of the dry season are all driven by the stochastic structure of rainfall, though λ and γ_Q are also affected by the soil, vegetation, and geomorphology of the catchment. These parameters can alternatively be estimated from streamflow or rainfall time series.

Using streamflow, the duration of the rainy season is estimated each year by fitting a step function to the streamflow time series (Figure 2a). T_d is then obtained by subtracting the median duration of the rainy season from 365. λ and $1/\gamma_Q$ are estimated by considering the subset S of rainy season days with a positive discharge slope (i.e., day t is selected if $Q_{t-1} < Q_{t+1}$) during the rainy season. We then have

$$\lambda = \frac{N_S}{T_d}, \quad (19)$$

$$1/\gamma_Q = \frac{1}{2N_S} \sum_{t \in S} Q_{t+1} - Q_{t-1} \quad (20)$$

where N_S is the length of S .

Using rainfall, λ_p can be estimated based on the frequency of rainy season precipitation, and then λ computed via equation (1), drawing on estimated evaporation potential and soil textural properties. The parameter γ_Q can be calculated from the mean intensity of rainfall events (equation (4)), combined with the catchment area and the estimated wet-season recession constant, k . T_d can be approximated by fitting a step function to rainfall time series instead of daily streamflow. The resulting dry season duration $T_{d,rain}$ slightly underestimates T_d (Table 1) as groundwater recharge causes a time lag between the onset of wet season rainfall and the associated flow response. In the catchments considered in our case study, this lag is

Table 1. Descriptive Statistics of Catchments by Region^a

	W. Australia	Nepal	California
	N = 6	N = 24	N = 8
<i>Catchments</i>			
Number of years	26 (15, 35)	19 (17, 22)	50 (33, 61)
Area (km ²)	306 (22, 802)	813 (512, 2380)	126 (110, 218)
Altitude range (m)	186 (179, 223)	4380 (3120, 6190)	921 (792, 1150)
Max snow cover (% area)	0 (0, 0)	16 (8, 32)	0 (0, 0)
Glaciated watershed	0% (0)	29% (5)	0% (0)
Intermittent flow	100% (6)	6% (1)	50% (4)
<i>Model Parameters</i>			
a ((m ³ /s) ^{1-b} d ^{2-b})	0.13 (0.12, 0.20)	33 (4.8, 9.5) (10 ⁻⁴)	0.036 (0.011, 0.052)
b	1.60 (1.44, 1.76)	2.40 (2.11, 2.51)	1.86 (1.81, 1.91)
k (d ⁻¹)	0.26 (0.19, 0.30)	0.16 (0.12, 0.19)	0.25 (0.19, 0.26)
λ (d ⁻¹)	0.33 (0.32, 0.34)	0.42 (0.40, 0.44)	0.24 (0.23, 0.25)
1/γ _Q (mm)	1.17 (0.64, 2.16)	28.7 (18.5, 60.2)	5.64 (3.48, 15.09)
T _d (d)	299 (295, 299)	280 (273, 286)	306 (305, 306)
<i>Gauged Rainfall</i>			
Annual Rain (mm)	821 (719, 925)	2170 (1630, 3230)	616 (479, 769)
λ _p (d ⁻¹)	0.52 (0.48, 0.55)	0.66 (0.62, 0.83)	0.48 (0.47, 0.49)
1/γ _p (mm)	10.30 (9.63, 10.56)	22.26 (16.87, 27.49)	10.35 (7.42, 13.04)
AR	0.34 (0.33, 0.36)	0.23 (0.17, 0.40)	0.40 (0.36, 0.44)
GS	0.86 (0.78, 0.96)	1.01 (0.86, 1.53)	0.74 (0.72, 0.75)
T _{d,rain} (d)	262 (255, 269)	279 (266, 286)	286 (281, 292)
CV _{T_w}	0.25 (0.19, 0.28)	0.20 (0.17, 0.23)	0.29 (0.27, 0.32)
<i>Model Performance (Estimated Based on Streamflow Input)</i>			
<i>Nash-Sutcliffe Coefficient of Log-Transformed Streamflow Quantiles</i>			
<i>Period of Record</i>			
Whole year	0.67 ^b (0.60, ^b 0.77 ^b)	0.90 (0.84, 0.92)	0.97 ^b (0.91, ^b 0.98 ^b)
Dry season	0.89 (0.86, 0.94)	0.15 (-0.50, 0.60)	0.65 (0.64, 0.73)
Wet season	0.43 ^b (0.22, ^b 0.60 ^b)	0.78 (0.61, 0.83)	0.95 ^b (0.84, ^b 0.96 ^b)
<i>AFDC</i>			
Median	0.65 ^b (0.58, ^b 0.77 ^b)	0.91 (0.84, 0.94)	0.94 ^b (0.92, ^b 0.96 ^b)
Upper CI90	0.23 ^b (0.18, ^b 0.62 ^b)	0.73 (0.67, 0.80)	0.60 (0.45, 0.65)
Lower CI90	0.77 ^b (0.76, ^b 0.88 ^b)	0.90 (0.85, 0.94)	-0.42 ^b (-5.15, ^b 0.40 ^b)

^aIn this table, Q_m (Q₂₅, Q₇₅) represent the lower quartile Q₂₅, the median Q_m, and the upper quartile Q₇₅ for continuous variables. N is the number of nonmissing values. Numbers after percents indicate the number of catchments. Model parameters are estimated from the observed hydrographs. Nash Sutcliffe coefficients are computed on flow quantiles 1/365 to 364/365.

^bIntermittent flow at one or more gauges: nonpositive flow quantiles are omitted.

correlated at the 99% confidence level to both aquifer storage characteristics (parameter *a*) and the duration *T_{d,rain}* of the dry season. Thus we estimate *T_d* from rainfall time series empirically by regressing linearly the lags *T_d* - *T_{d,rain}* against *T_{d,rain}* and *a*, which estimation method is provided below.

$$T_d = T_{d,rain} + h_0 + h_{T_{d,rain}} T_{d,rain} + h_a a \tag{21}$$

where *h₀* = -129.13, *h_{T_{d,rain}}* = -0.47, and *h_a* = 146.49 are the ordinary least squares coefficients of the regression (*R*² = 0.53).

2.3. Recession Parameters

Due to the multiplicity of flow generation processes concurrently represented in a hydrograph, the empirical determination of recession parameters from streamflow time series is a significant challenge and an active field of research [see e.g., Tallaksen, 1995; Nathan and McMahon, 1990; Stoelzle et al., 2013].

Here, we estimate the wet-season recession constant *k* by (i) identifying all recessions (consecutive days of decreasing streamflow) longer than 4 days during the rainy season and (ii) estimating the parameters of equation (9) by regressing the logarithm of the discharge against time for each recession segment [Tallaksen, 1995]. The recession constant is then obtained by taking the median value of the recorded slope coefficients of the regression.

Dry-season recession constants *a* and *b* are calibrated stochastically based on equation (11). The initial condition *Q₀* is estimated each year as the streamflow value at the last peak before the end of the wet season

identified by the fitted step function. The estimates of a and b that minimize the sum of squared errors between the modeled (equation (11)) and observed dry season base flow across all years are determined numerically through simulated annealing [Bélisle, 1992]. Due to the low frequency of rainfall and overwhelming dominance of base flow in the dry season, the estimation of a and b through this method appears to be robust to the choice of base flow separation method—here the Lyne Hollick algorithm [Nathan and McMahon, 1990]. The more direct method of regressing the log-transformed rate of change of discharge against the log-transformed base flow [e.g., Brutsaert and Nieber, 1977; Ceola et al., 2010] resulted in biased estimates of a and b in our case study because the discharge rate is not detectable on a daily scale on a substantial part of the recession.

Alternatively, because the wet-season recession constant k and the dry-season recession parameters a and b describe the same watershed, they must be related. For consistency between long and short recession behavior, we require that the power-law recession (left-hand side of equation (22)) be approximated by an exponential recession (right-hand side of equation (22)) for sufficiently short recession times t :

$$(q_0' - art)^{\frac{1}{r}} = q_0 e^{-kt} \tag{22}$$

Substituting $q_0 = E[Q_0]$ (equation (8)), the expected value of flow peaks, and $t = 1/\lambda$, the mean duration of recessions during the wet season into equation (22), we solve for a :

$$a = \frac{\lambda}{-r} (e^{\frac{-r}{\lambda}} - 1) \left(\frac{m+1}{\lambda Q} \right)^r \tag{23}$$

In the analysis, k is estimated independently from a and b using equations (9) and (10). However, we test the ability of equation (23) to reproduce the obtained estimate of a in section 3.1.

2.4. Evaluation Metric

Following *Castellarin et al.* [2004b], we compare analytical and empirical FDCs using the Nash-Sutcliffe Coefficient (NSC) applied to the flow quantiles:

$$NSC = 1 - \frac{\sum_{j=1}^{350} (\hat{q}_j - q_j)^2}{\sum_{j=1}^N \left(q_j - \frac{1}{N} \sum_{j=1}^{350} q_j \right)^2} \tag{24}$$

where \hat{q}_j and q_j are the empirical and analytical daily streamflows associated with quantile j .

Castellarin et al. [2004b] use NSC intervals ([0.75, 1]: good, [0.5, 0.75]: fair, $[-\infty, 0.5]$: poor) to evaluate FDC regionalization methods at ungauged sites. Although this study does not consider ungauged catchments, we use the above intervals as benchmarks to quantify the performance of the model. In order to mitigate the outlier effect of large floods, we take the logarithm of the flow quantiles before computing the NSC. Note that although representative of the overall modeling performance, the NSCs are not necessarily representative of the model's utility in the context of a specific application, which hinges on its ability to predict the duration of particular flows that are exogenously determined by design constraints (e.g., the design flow Q_d in the case of run-of-river hydropower). Therefore, we use error-duration curves [Pugliese et al., 2013] to assess the repartition of the errors across flow quantiles. The curves represent the median 40% and 80% empirical confidence interval of the relative residuals of streamflow values against their duration.

2.5. Numerical Analysis

Rainfall in several seasonally dry climates does not always follow a Poisson process [Katz and Parlange, 1996; Müller and Thompson, 2013]. Similarly, many watersheds exhibit nonlinear recession behavior, which indicates a nonexponential travel time distribution. We evaluate the robustness of the FDC model to the violation of these two assumptions through a numerical analysis, in which we generate streamflow data by

routing non-Poissonian synthetic rainfall through a nonlinear water table and compare the resulting FDCs to those obtained using equation (3).

To generate synthetic streamflow, we first generate synthetic rainfall time series in which rainfall occurrence is more or less autocorrelated, and in which rainfall intensities follow a gamma distribution [Müller and Thompson, 2013]. By forcing the first-order autocorrelation parameter (AR) to 0, and the shape parameter of the gamma distribution (GS) to 1, these assumptions can replicate a Poisson Process. The synthetic rainfall forces a vadose zone soil moisture balance model with linear losses to evapotranspiration [Botter et al., 2007a; Porporato et al., 2004]. The resulting water table recharge R replenishes a nonlinear water table yielding a runoff Q described by Kirchner [2009]

$$\frac{d(\ln(Q))}{dt} = aQ^{b-2} \left(\frac{R}{Q} - 1 \right), \quad (25)$$

where a and b are nonlinear recession parameters (equation (10)). This initial value problem was solved numerically with the *Isodes* solver [Soetaert et al., 2010].

We test the model's robustness to non-Poissonian rainfall and nonexponentially distributed response times (Hypothesis H1) by (i) generating a 10,000 day long synthetic streamflow record, (ii) estimating the parameters k , λ , and γ_Q from the synthetic time series, (iii) constructing the empirical FDC from synthetic streamflow, and (iv) comparing it to the analytical FDC (equation (3)) computed from the estimated parameters. The Poissonian character of rainfall was progressively eroded by altering the first-order autocorrelation coefficient on rainfall occurrence (AR) away from 0 within the $[-0.3, 0.7]$ range. The exponential character of the rainfall intensity distribution was progressively eroded by altering the shape parameter (GS) away from 1 within the $[0.02, 2]$ interval. Nonlinearity was investigated by increasing the exponent b of the recession relation from 1 (i.e., the linear case of exponentially distributed travel times) to a maximum value of 3. The effects of both non-Poissonian rainfall and nonlinear water table recessions on the streamflow FDC are expected to decrease with increasing rainfall frequency, and λ_p was therefore varied in the range $[0.2, 0.8]$.

We also assessed the robustness of the model to random interannual variations in T_w , the duration of the wet season, by simulating 30 years of streamflow over 1000 Monte Carlo runs. At each run, 30 instances of T_w are drawn from a gamma distribution with a given mean (μ_{T_w}) and coefficient of variation (CV_{T_w}). Wet-season streamflow time series of length T_w are then generated for each year as described above, and a nonlinear recession of length $365 - T_w$ is finally appended to each year's simulated wet season. Modeling performance is evaluated by computing the NSC of the modeled PoRFDC, median AFDC and 5th percentile AFDC (which all assume a constant T_w) against corresponding simulated streamflow distributions. We investigate the effects of fluctuations in the mean and variability of T_w by varying μ_{T_w} in the $[40, 120]$ interval and CV_{T_w} in the $[0, 4]$ interval—the further CV_{T_w} is from 0, the larger the random interannual variations in the duration of the wet season.

2.6. Case Studies

We rely on observed streamflow data to evaluate whether dry-season streamflow PDF can be constructed from a deterministic recession relationship with a stochastic initial condition (Hypothesis H2). We used daily streamflow observations from 24 catchments in Nepal (Nep) [HKH-FRIEND, 2011; Department of Hydrology and Meteorology, 2011], 8 in Coastal California (CA) [United States Geological Survey, 2013], and 6 in Western Australia (WA) [Department of Water, 2013] with between 11 and 76 (mean: 18) years of daily streamflow records. The location of the gauges is shown in Figure 1, and Table 1 provides a summary of the relevant catchment characteristics and rainfall statistics from daily rainfall time series recorded by precipitation gauges [HKH-FRIEND, 2004; Department of Hydrology and Meteorology, 2011; California Irrigation Management Information System, 2013; Bureau of Meteorology, 2013] closest to the catchment centroids. Nepalese watersheds are subject to the seasonality of the Indian Summer Monsoon and to the complex topography and variable soil depths of the Central Himalayas. Californian and Southwestern Australian watersheds are subject to a highly seasonal Mediterranean climate with significant winter precipitation. While Californian watersheds are characterized by shallow soils and complex topography, Australian catchment are flat with deep soils.

Table 2. Rainfall-Estimated Catchments^a

	Khimti Kohla (K)	Modi Kohla (M)	Ellenbrook (E)
<i>Catchments</i>			
Location	Nepal	Nepal	W. Australia
N_{yr}	30	21	38
Area (km ²)	310	142	581 (90)
Z_{Rge} (km)	3.8	4.5	0.2
Snow (%)	12.1	6.5	0.0
AI	1.92	2.87	0.34
Interm. (d/yr)	0	0	142
P_{yr} (mm/yr)	2230	3350	653
λ_p (d ⁻¹)	0.90	0.91	0.49
γ_p^{-1} (mm)	18.8	28.9	8.3
AR	0.23	0.51	0.33
GS	1.09	1.23	0.76
$T_{d,rain}$ (d)	277	286	252
CV_{r_w}	0.19	0.19	0.24
<i>Model Parameters</i>			
a ((m ³ /s) ^{1-b} d ^{2-b})	0.00089	0.0015	0.129
b	2.09	2.14	1.78
k (d ⁻¹)	0.11	0.18	0.30
λ (d ⁻¹)	0.44	0.44	0.34
γ_Q^{-1} (mm)	18.9	14.1	2.3
T_d (d)	276	285	300
<i>Model Performance (Estimated Based on Precipitation Input)</i>			
<i>Nash-Sutcliffe Coefficient of Log-Transformed Streamflow Quantiles</i>			
<i>Period of Record</i>			
Whole year	0.97	0.95	0.69 ^b
Dry season	0.92	0.85	0.22 ^b
Dry season base flow	0.97	0.93	0.77 ^b
Wet season	0.83	0.93	0.82
<i>AFDC</i>			
Median	0.98	0.96	0.70 ^b
CI90 (top)	0.75	0.76	0.05 ^b
CI90 (bottom)	0.96	0.99	0.72 ^b

^aIn this table, N_{yr} is the number of complete years with available observations, Z_{Rge} the altitude range of the catchment, D_{RnGge} the distance between the catchment centroid and the nearest rain gauge, $Snow$ the maximum snow covered area ratio, AI is the aridity index P/PET , $Interm$ the average number of days per year without flow and P_{yr} is the mean yearly rainfall, λ_p is the rainfall frequency during the wet season and γ_p the inverse of mean rainfall intensity. AR is the first-order autocorrelation coefficient of rainfall occurrence, GS is the shape parameter of a gamma distribution fitted on rainfall intensity, $T_{d,rain}$ the median dry season duration estimated from precipitation time series, and $SD(T_{d,rain})$ its standard deviation. Model parameters are estimated based on gauged rainfall, assuming actual evapotranspiration values of 2.1 mmd⁻¹ (Nepal) and 1.6 mmd⁻¹ (W. Australia), and soil moisture capacities of 16 mm (Nepal) and 150 mm (W. Australia). The approximate catchment area effectively contributing to the Ellenbrook streamflow is given in parenthesis. Nash Sutcliffe coefficients are computed on flow quantiles 1/365 to 365/365. The model performance reported for Ellenbrook is based on the 90 km² of catchment contributing to streamflow, not the 581 km² topographic watershed.

^bIntermittent flow: nonpositive flow quantiles are omitted.

The modeling approach is tested by comparing empirical PoRFDCs and the median and 90% empirical confidence interval on AFDCs generated from dry season streamflow to their analytical counterparts. Because the main stochastic driver of dry season streamflow (Q_0) is an annual random process, the evaluation of AFDCs is done on the gauges with more than 20 years of available data. Empirical PoRFDCs (using both wet and dry season streamflows) are finally compared to their analytical counterparts.

The predictive ability of the method is assessed by reproducing the above analyses using rainfall (instead of streamflow) data to estimate λ and γ_Q . In order to limit the effect of spatial rainfall heterogeneities, which can be significant in the Himalayas [Müller and Thompson, 2013], the rainfall-based parameters are computed for a subset of three catchments (two in Nepal and one in Western Australia) that are small and where the catchment centroid is close (<20 km) to a rainfall gauge (Table 2).

2.7. Application: Estimation of Electricity Production Using Flow Duration Curves

One final analysis was conducted to illustrate the potential value of the modeling approach for infrastructure design, including an analysis of error not only in the FDC itself, but in the propagation of any such errors into infrastructure design criteria. Flow durations have a direct impact on energy production from run-of-river hydropower facilities. The energy produced by a hydropower plant in a period T is the time integral of instantaneous power generated from the available discharge:

$$E = \rho g H \int_0^T \eta(Q^*) Q^*(D) dD \quad (26)$$

where ρ is the density of water and g the acceleration due to gravity. H is the (assumed constant) net hydraulic head drop across the turbine. $Q^*(D)$ is the average discharge passing through the turbines on day D and is related to the FDC $Q(D)$, the design capacity Q_{DC} and the minimal flow discharge prescription MDF [Basso and Botter, 2012].

$$Q^*(D) = \begin{cases} Q(D) - MDF, & \text{if } Q(D) - MDF < Q_{DC} \\ Q_{DC}, & \text{otherwise} \end{cases} \quad (27)$$

The streamflow effectively used to generate electricity is thus bounded by the design capacity of the turbine. Predicting electricity production therefore requires correctly estimating by the duration of the lower quantiles (i.e., $Q(D) < Q_{DC}$) of the FDC. Turbine efficiency $\eta(Q^*)$ may be modeled as a step function with constant value of η_T above a discharge threshold $\alpha_T Q_d$, below which no electricity is produced. If N such turbines are combined, the plant will have an overall design flow of $N \cdot Q_{DC}$ and will function with an efficiency of η_T for flows above $\alpha_T \cdot Q_{DC}$.

Table 3 displays the design parameters of two hydropower plants located directly downstream of the Nepalese streamflow gauges included in the analysis in Table 2. The practical relevance of the FDC model derived here is tested by propagating the modeling errors from FDCs to electricity production estimates. First, the long-term annual electricity production is evaluated based on the period-of-record analytical FDC determined from rainfall parameters, and compared to production estimates based on empirical FDC. The (rainfall estimated) median AFDC and the lower bound of the 90% CI are then used to estimate the electricity production in a typical and particularly dry year.

3. Results

3.1. H1: Numerical Analysis

Results from the Monte Carlo analysis are presented in Figure 3, showing the outcomes of the three numerical experiments described in section 2.5.

With Nash Sutcliffe coefficients (NSC) above 0.97 within the range of parameters encountered in our case studies (i.e., $\lambda_p > 0.4$, $GS > 0.7$, $AR \in [0, 0.5]$), the first experiment showed that non-Poissonian rainfall has a negligible effect on the model's ability to reproduce wet season streamflow (Figures 3a and 3d). With effects on the NSC below 0.1, autocorrelated rainfall occurrence has little effect on model performance, especially for high rainfall frequencies. Gamma distributed (rather than exponentially distributed) rainfall intensities significantly affect the model performance for shape factors < 0.5 , as NSC tends toward $-\infty$ when GS tends toward 0.

In line with Ceola *et al.* [2010], the second experiment (Figure 3b and e) showed that nonexponentially distributed water table travel times have a significant effect on the model performance. The effect was especially visible when the power coefficient b was above 2, denoting a hyperbolic storage-discharge relation [Kirchner, 2009]. However, as hypothesized in section 2.1.3, the effect of nonlinearities decreased with increasing rainfall frequency. Although most catchments are characterized by $b > 2$ (Table 1), the high frequency of rainfall allowed modeling the catchments as linear reservoirs during the rainy season, resulting in a good match ($R^2 = 0.92$) between the nonlinear recession parameters a obtained from equation (23) and the corresponding empirically estimated values of a (Figure 2d).

The third experiment showed that within the range of seasonality parameters encountered in our case studies (i.e., $CV_{T_w} < 0.5$ and $\mu_{T_w} \in [60, 100]$), stochastic variations in the duration of wet seasons do not have a significant impact on the performance of the any of the FDC models. The lower-quantile-AFDC (filled symbols in Figure 3f) appears more sensitive to random variations in T_w which affect modeling performance for CV_{T_w} values as low as 0.5 at a mean T_w of 40 days. In all the other considered cases (median AFDC, PoRFDC), variations in T_w only seem to have a significant effect on the modeling accuracy for CV_{T_w} values above 1.

Table 3. Design Parameters and Electricity Production Estimates of Two Nepalese Run-of-River Hydropower Plants^a

	P (MW)	QDC (m ³ s ⁻¹)	H (m)	Turbine	Observed (GWhy ⁻¹)			Modeled (GWhy ⁻¹)		
					PoR.	AFDC		PoR.	AFDC	
						Median	5th%		Median	5th%
Khimti 1	60			5xPelton : $\eta_T=0.82$ $\alpha_T=0.24$	409	409	338	391	393	379
Modi	13	26	67	2xFrancis : $\eta_T=0.75$ $\alpha_T=0.05$	53.8	53.5	45.9	46.0	47.0	41.0

^aThe observed production is computed from observed streamflow records. The modeled production is estimated using the analytical flow duration curve models based on rainfall records. The long term, median, and 5th percentile annual productions are calculated based on the PoRFDC, and median and 5th percentile AFDC, respectively. The assumed minimum flow discharged (MFD) is 0.5 m³s⁻¹.

3.2. H2: Case Studies

3.2.1. Hydrograph-Based Analysis

Nash-Sutcliffe coefficients for FDCs from the 38 catchments are presented in Table 1, using direct hydrograph observations to estimate the model parameters λ and γ_{Qr} , and thus excluding errors introduced by precipitation observation and the vadose zone model parameterization. The corresponding error-duration curves, which display the repartition of the relative errors across flow durations, are presented in Figure 4.

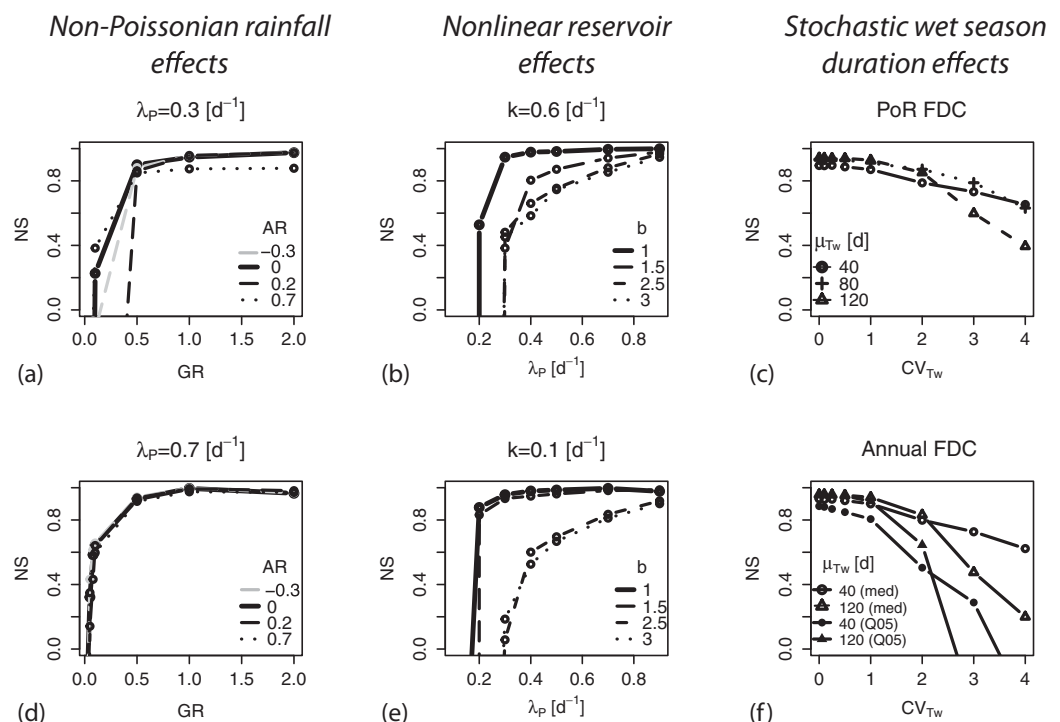


Figure 3. Results of Monte Carlo analyses showing the (a and d) effects of non-Poissonian rainfall and (b and e) nonexponentially distributed water table response times on the model performance (as measured by the NSC) for wet season streamflow. The effect on model performance for (c) stochastic wet season duration on PoRFDCs, median (f) AFDC (white symbols) and 5th percentile AFDC (Figure 3f, black symbols). Default parameters: $A=6500\text{km}^2$, $ETP=3.5\text{mm} \cdot \text{d}^{-1}$, $nZ_r(s_1-s_w)=180\text{mm}$, $\gamma_p=0.06\text{mm}^{-1}$, $\lambda_p=0.73\text{d}^{-1}$, $k=0.6\text{d}^{-1}$, $b=1$, $AR=0$, $GS=1$.

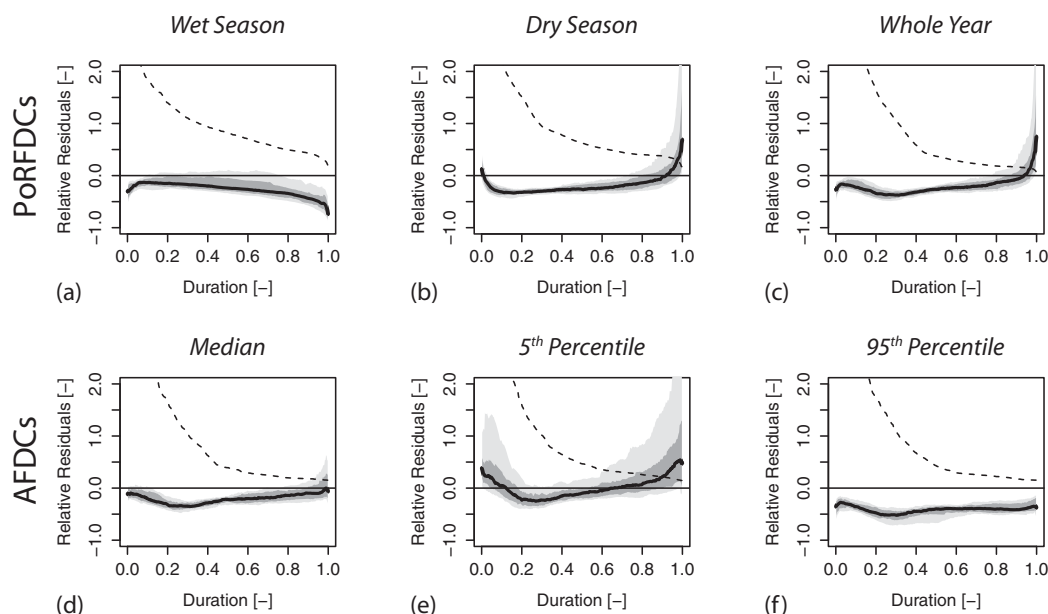


Figure 4. Error-duration curves. The thick line represents the median of the relative error for a given streamflow duration across all sites. The dark and light gray nested bands contain 40% and 80% of the relative errors, respectively. The hashed line is the median FDC normalized by the mean discharge. PoRFDs for the (a) wet season, (b) dry season, and (c) whole year. AFDCs for (d) the median, (e) the 5th percentile, and (f) the 95th percentile.

Most period-of-record FDCs are well reproduced by the model with median logNSC above 0.65. With a median logNSC of 0.43, the wet season in Nepal is a notable exception. There the fit is significantly better on high flow (nonlog transformed NSC = 0.79). The observed underestimation of low flows (Figure 4a) can be attributed to a strong deviation from the exponential response time assumption in Nepalese basins (median $b = 2.40$). Yet the errors generally do not propagate to nonseasonal FDCs because dry season streamflow is driven by the last wet season peak, which appears to be well estimated, as seen on Figure 4b at duration 0. A second exception to the generally good PoRFD estimates arises for the dry-season FDC in WA (median logNSC = 0.15). With a median (nonlog transformed) dry-season NSC of 0.70, the poor performance in WA is explained by the intermittent nature of the streams and the exaggerated impact of very low flows on the logNSC.

Predictions of the median dry-season AFDC overall were good with median logNSC above 0.64. With a median logNSCs of 0.75, the lower bound of the 90% CI was well reproduced in Nepal and WA, but not CA, where flow quantiles were overestimated (and caused the large spread of error observed in Figure 4e). The model reproduced the upper bound of the 90% CI with median logNSC > 0.6 in Nepal and California and a median logNSC dropping to 0.23 in WA.

3.2.2. Rain-Based Analysis

The FDCs related to Khimti (Nepal) and Ellenbrook (WA), the two catchments selected for the rain-based analysis are presented in Figure 5. Unlike the results summarized in Table 1, the parameters T_d , λ , and γ_Q of the analytical FDCs were calculated from the seasonality, frequency and intensity of gauged rainfall, taking locally reported values for actual evapotranspiration and available soil moisture capacity (Table 2). The examples in Figure 5 were selected to illustrate model performance for a subset of catchments deviating from standard model assumptions: (1) FDC estimation in a nonhomogeneous, arid catchment; (2) Effects of poorly marked seasonality with significant dry season rainfall, and (3) Spatially heterogeneous rainfall. We explore the consequences of these deviations and some opportunities to adapt the simple model.

Example 1 concerns FDC estimation in arid catchments, as exemplified by Ellenbrook (WA) (Figures 5e–5h). There, the overestimation of wet season streamflow (Figure 5e, dotted line) is likely attributable to

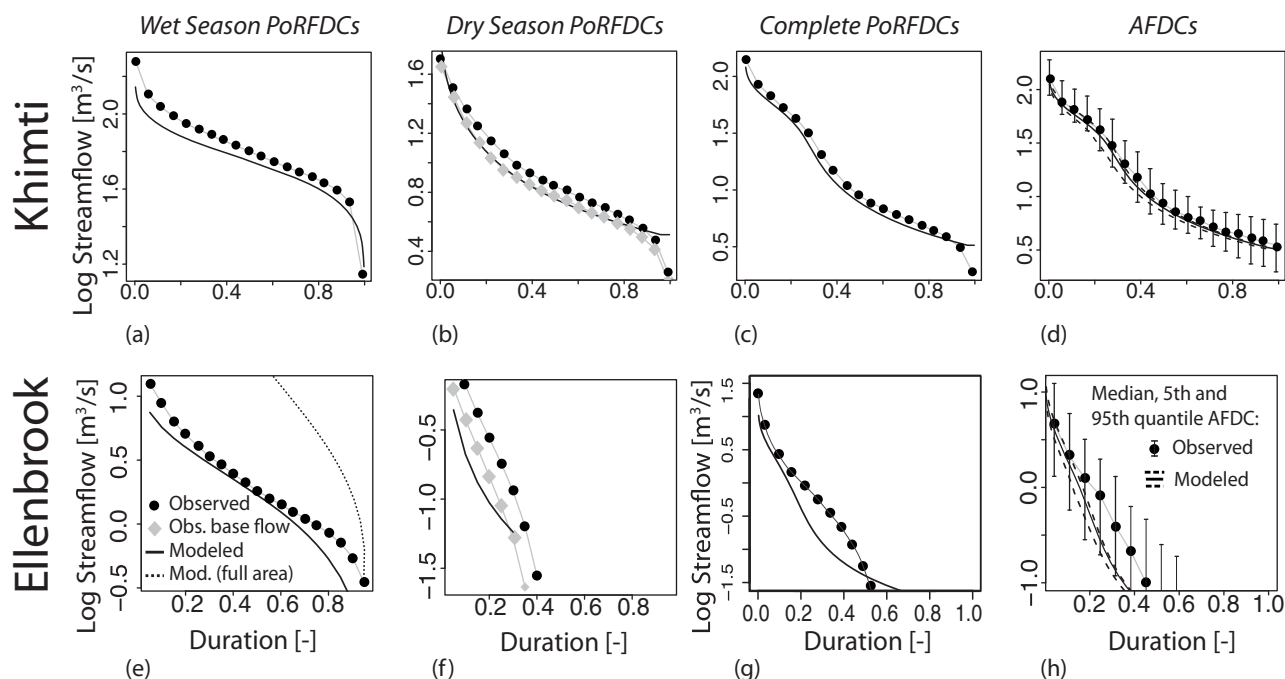


Figure 5. Empirical and analytical flow duration curves at (a–d) Khimti, Nepal and (e–h) Ellenbrook, Western Australia. PoRFDCs are given for the wet (Figures 5a and 5e) and dry (Figures 5b and 5f) seasons, and for the whole year (Figures 5c and 5g). Median, 5th and 95th quantile AFDCs are displayed in Figures 5d and 5h. The modeled wet season curve at Ellenbrook (Figure 5e) represents the analytical FDC obtained from rainfall over 1/5 of the topographic catchment area—the corresponding FDC over the whole catchment area is given in dotted lines. Gray diamonds in Figures 5b and 5f represent the empirical FDC obtained from dry season recessions filtered using the Lyne-Hollick base flow separation algorithm [Nathan and McMahon, 1990].

geological heterogeneities in a catchment where a significant proportion of the catchment area recharges groundwater rather than contributing to surface flow [Barron et al., 2009]. Reducing the modeled catchment area to the 20% of the catchment thought to supply the majority of base flow [Barron et al., 2009] increased the model performance dramatically (solid line).

Example 2 concerns the assumptions that no runoff occurs during the dry season. This leads to an underestimation of the duration of high flows during the dry season in locations poorly marked rainfall seasonality. This effect is particularly visible in Ellenbrook (WA) (Figure 5f), where the underestimation of dry season streamflow propagates to the PoRFDC. However, if the model output is compared to base flow (gray diamonds) rather than total flow (black dots) then the performance metrics drastically improve in both catchments (Figures 5b and 5f). This assumption may also explain the underestimation of the higher bound of the 90%CI of the AFDCs (Figures 5e and 5h): dry season precipitation is likely to occur in particularly wet years. Conversely, dry season precipitation is less likely to occur in particularly dry years, leading to the improved fits for the lower-quantile-AFDC.

The final example relates to the misestimation of parameters in areas with spatially heterogeneous rainfall, which likely explains the underestimation of wet season flows in Khimti by rainfall-estimated parameters (Figure 5a). While the model performs well for streamflow-derived statistics, estimating catchment-averaged rainfall parameters from rain gauge observation is challenging because of the complex topography [Müller and Thompson, 2013].

Despite these limitations, the analytical FDCs derived from rainfall-estimated parameters reproduced their empirical counterparts well, with most logNSCs above 0.75 (Table 2). In particular, while neglecting snow-melt contribution, the model performed well for all the FDC types at Khimti ($\logNSC > 0.75$) despite significant snow/ice cover (12%). The model was also able to reproduce specific hydrologically significant quantiles like the change in streamflow regime, visible at a duration of 0.3 on the PoRFDC and median AFDC in Khimti (Figures 5c and 5d), and the duration of the absence of flow during the dry season in Ellenbrook (Figure 5f). Finally, the estimation method (hydrograph or rainfall) had little overall impact on the good performance of the model.

3.3. Application: Estimation of Electricity Production Using Flow Duration Curves

Electricity production estimates for the two Nepalese hydropower plants are presented in Table 3. The long-term average, median, and 5th quantile of the annual power production are estimated using empirical FDCs (*Observed Prod.*). These empirical results are then compared to the corresponding values obtained from the analytical FDCs (*Modeled Prod.*) based on parameters estimated using rainfall time series. Electricity production is generally underestimated for the catchments (particularly at Modi Kohla). This is related to the underestimation of the duration of high flows (Figure 5a) caused by the lower seasonality of the region, which experiences pre and post-Monsoon storms. Conversely, electricity production is overestimated on dry years (5th percentile) at Khimti Kohla because from the inability of the model to reproduce the low flow conditions of the stream in dry years, when low discharge prevents generation for 2 weeks. This error source is amplified when considering production variability, that is the difference in production between a typical (i.e., median) and dry (i.e., 5th percentile) year. The error on production variability reaches 80% in Khimti and 30% at Modi. Overall, however, the predictions of annual power production were excellent, with errors below 15% for long-term average production and below 12% for annual production quantiles.

4. Discussion

4.1. H1: The Wet-Season FDC Model Is Robust to Deviations From Key Underlying Assumptions

Although the derivation of the original model relies on exponentially distributed response times, rainfall intensities and rainfall interarrival times, our results show that predictions of wet-season streamflow PDFs are relatively robust to small deviations from these assumptions. Yet the combination of hyperbolic storage-discharge relationships and low rainfall frequency reduced the model predictive ability. This situation arises in the strongly nonlinear recessions in Nepal, where the model overestimates the flashiness of wet season recession. There, this effect was nonetheless mitigated by the high rainfall frequency occurring during the ISM and had little effect on modeling accuracy beyond the wet season.

The assumption of a spatially heterogeneous watershed was violated in Ellenbrook (WA) in which regions with a sandy geology do not generate streamflow. With known geology, these effects could be satisfactorily corrected by adjusting the contributing area of the watershed.

Finally, the challenges associated with estimating catchment-scale effective rainfall statistics is illustrated by the case of Khimti (Nep), in which the model performs well for streamflow-derived statistics, but cannot reproduce these statistics based on the single rain gauge measurement in the topographically complex Himalayan catchment.

Thus, the modeling approach performs well in gauged basins, and holds promise for future application to ungauged basins.

4.2. H2: The Dry-Season FDC Can be Modeled as a Deterministic Recession Relationship With a Stochastic Initial Condition

We modeled dry season streamflow as an annual stochastic process driven by the intensity of the previous wet season and subject to a deterministic recession. Empirical dry-season FDCs in our case studies suggest that this simple model captures key flow behavior in seasonally dry regions. The high rainfall seasonality characteristic of these regions is a key prerequisite for the model to be applicable, as evidenced by its poorer performance during the dry season at Ellenbrook (WA). There, a 48 day lag has been observed between the beginning of wet season precipitation and a persistent streamflow rise. Runoff increments during that time lead to the underestimation of high flows during the dry season.

While numerical simulations have shown that the model is robust to fluctuations in the timing and duration of the wet season, unaccounted fluctuations in the frequency and intensity of dry season storms affects modeling performance in watersheds with weaker rainfall seasonality. This, along with the likelihood that during extreme rainfall events flow generation processes bypass the water table, also explain the model's poor prediction of the higher CI bound on the AFDCs.

Generally, qualitative results (Figure 2) and the overall good modeling performance on long term and annual FDCs support the utility of the proposed model and point toward water table discharge as the main mechanism for dry-season flow production in the considered catchments. Intra-annual flow variations are

deterministically driven by the water table, while interannual variations are stochastically forced by wet season rainfall. In the Nepalese context, this supports previous findings [Andermann *et al.*, 2012] pointing toward the storage in the fractured bedrock and subsequent release of large volumes of water from the previous monsoon as a key flow generation mechanism. Unlike existing models for seasonally dry climates [e.g., Rianna *et al.*, 2013; Pumo *et al.*, 2013], where an atom of probability associated to zero flow is assigned to the entire dry season, our approach allows accounting for that important mechanism. In Nepal, integrating such a seasonal recession in our model improved the median NSC on period-of-record FDCs by 0.18, compared to an alternate model where a constant dry season flow of zero was assumed. Our results also support the conclusion that the contribution of snow and glacial melt to streamflow variability is small in the Central Himalayas—up to 10% of the streamflow volume according to Chalise *et al.* [2003].

Although the method allowed FDCs to be modeled in relatively dry areas like California, modeling discharge in arid climates remains a significant challenge [Castellarin *et al.*, 2013]. Under such conditions, temporal shifts and/or spatial heterogeneities can have a very significant effect on streamflow. Thus the Ellenbrook catchment (WA), where local geological conditions affect the ability of the hillslope to generate streamflow [Barron *et al.*, 2009] and where a 20% decline in rainfall since 1970 has led to a 65% decline in average streamflow [Thompson *et al.*, 2013a], likely represents a limiting case with respect to the applicability of the proposed model in arid catchments. Nonetheless, period-of-record FDCs were successfully modeled at all locations with most median NSC coefficients above 0.75—the *good fit* benchmark of 0.75 in Castellarin *et al.* [2004].

4.3. Practical Relevance

Being able to estimate the inter and intra-annual variation of streamflow has considerable practical importance, notably to inform water resources and ecosystem management policies [Richter *et al.*, 1997, 2003] and hydropower operations. This was particularly evident in the run-of-river power generation case study, where electricity production can decrease by up to 20% in dry years, potentially affecting the short term financial sustainability of the infrastructure. Our analysis of two Nepalese run-of-river power plants has shown that a significant fraction of the interannual variation of electricity production can be reproduced using rainfall statistics and recession constants to model the interannual variability of wet season streamflow. The model allows the ensuing cash-flow variability to be accounted for during the design phase of the infrastructure, which is currently typically based on period-of-record FDCs and assumes constant annual revenues [e.g., Hosseini *et al.*, 2005; Santolin *et al.*, 2011; Basso and Botter, 2012].

A further advantage offered by the process-based nature of the model lies in its ability to disentangle the effects of changes in climate and landscape on streamflow dynamics. The proposed approach offers an appealing alternative to extend to seasonally dry climates existing models relating catchment storage dynamics to nutrient transport [e.g., Basu *et al.*, 2011], landscape characteristics (riparian width) [e.g., Muneepeerakul *et al.*, 2007] or ecological dynamics (plant pathogen risks) [Thompson *et al.*, 2013b].

Finally, although not explicitly addressed in this study, the model offers a promising approach to the regionalization of FDCs to ungauged catchments because it relies on a limited number of physically observable parameters. Many of these parameters (e.g., catchment areas, rainfall, evapotranspiration, soil type) are directly and globally available as gridded data sets. However, the study also showed that the model is sensitive to spatial heterogeneities in catchment characteristics and to the accurate computation of catchment-scale rainfall statistics. These effects, in addition to the propagation of errors from gridded data sets, on the model's performance in ungauged catchments are yet to be assessed. Nonetheless, as indicated by the excellent estimation of run-of-river hydroelectricity production, the modeling approach is apparently well suited to support large-scale site suitability analysis for water infrastructure development [e.g., Yi *et al.*, 2010; Kusre *et al.*, 2010; Larentis *et al.*, 2010; Lee *et al.*, 2008].

5. Conclusion

In this study, we derived an analytical expression for the FDC of streams in seasonally dry climates. The approach can be successfully applied in a wide range of conditions that are observed in seasonally dry climates and is relatively robust to deviations from the assumptions utilized in the development of the model theory. The process-based nature of the proposed model offers numerous

advantages, including small data and calibration requirements and the ability to incorporate changes in climate and landscape properties into the predictive framework. These advantages, along with the ability to disentangle interannual and intra-annual variations of low flows offer considerable scope to use this low dimensional modeling approach to inform infrastructure design and water resources policies.

Appendix A: Derivation of the Dry-Season Streamflow CDF

The CDF of dry-season streamflow Q_d is derived using the law of total probabilities

$$P_{Q_d}(q_d) = P\{Q_d \leq q_d\} = \int_{Q_0} P_{Q_d|Q_0}(q_d, q_0) p_{Q_0}(q_0) dq_0 \tag{A1}$$

where Q_0 is the random variable representing streamflow at the beginning of the dry season.

Streamflow in any given dry season is bounded by its value at the start and at the end of the season because the receding streamflow is a decreasing function of time. The conditional CDF $P_{Q_d|Q_0}$ is therefore a piece-wise function taking the value of one for flows greater than Q_0 and of zero for flows below $Q_d(T_d, q_0)$. We first provide a detailed analysis of the bounds of the domain of $P_{Q_d|Q_0}(q_d)$ in the case of a power-law recession and then describe the integration of equation (A1) to obtain the unconditional CDF of dry season streamflow.

A1. Bounds of the Conditional Streamflow CDF

We examine the conditional streamflow CDF $P_{Q_d|Q_0}(q_d)$, that is the probability that the discharge governed by the deterministic recession:

$$Q_d(t) = (q_0^r - art)^{\frac{1}{r}} \tag{A2}$$

falls below an arbitrary threshold q_d during a recession period T_d . Three regions of q_0 are immediately apparent (Figure A1) and result in the three pieces of the conditional CDF.

1. In the first region all streamflow values during the dry season ($t \in [0, T_d]$) lie *below* q_d for a given initial flow q_0 , therefore

$$P_{Q_d|Q_0}(q_d, q_0) = 1. \tag{A3}$$

This situation arises if

$$q_0 < q_d \tag{A4}$$

because $Q_d(t)$ is strictly decreasing.

2. In the second region all streamflow values during the dry season lie *above* q_d for a given initial flow q_0 , therefore

$$P_{Q_d|Q_0}(q_d, q_0) = 0. \tag{A5}$$

Again, because $Q_d(t)$ is strictly decreasing, this situation arises for

$$q_0 \geq (q_d^r + arT_d)^{1/r} \tag{A6}$$

However, if $r < 0$ then the values taken by streamflow at the end of the dry season must lie beneath an upper bound:

$$\max_{q_0} Q_d(T_d) = \lim_{q_0 \rightarrow \infty} Q_d(T_d) = (-arT_d)^{1/r} \tag{A7}$$

Therefore, this second region does *not* exist (for any value of q_0) if $q_d > (-arT_d)^{1/r}$ and $r < 0$.

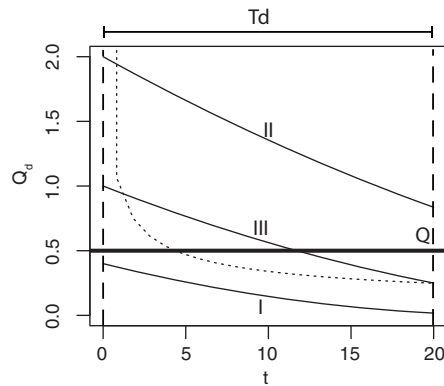


Figure A1. Regions of $P_{Q_d \leq Q|Q_0}$. If $Q_d(0) \leq Q$ (curve I) all values of $Q(t)$ are below Q and $P_{Q_d \leq Q|Q_0} = 1$. If $Q_d(T_d) > Q$ (curve II), all values of $Q_d(t)$ are above Q and $P_{Q_d \leq Q|Q_0} = 0$. In all other cases (e.g., curve III), $Q_d(t)$ crosses Q during the dry season and $-r \frac{\partial p}{\partial x_i} + \frac{\partial}{\partial x_j} \varepsilon \eta \left(\frac{\partial u_j}{\partial x_i} + \frac{\partial u_i}{\partial x_j} \right) - f = 0$. If $r < 0$ and $Q > (-arT_d)^{1/r}$ (dotted line) $Q_d(t)$ crosses Q during the dry season for any initial streamflow value, and region 2 (i.e., $P_{Q_d \leq Q|Q_0} = 0$) does not exist.

the bounds of the 3 regions described above. If $r < 0$ and $q_d > (-arT_d)^{1/r}$, the second region does not exist and equation (A1) integrates as:

$$P_{Q_d}(q_d) = P\{Q_d \leq q_d\} = \int_0^\infty P_{Q_d|Q_0}(q_d, q_0) p_{Q_0}(q_0) dq_0$$

$$= \int_0^{q_d} 1 \cdot p_{Q_0}(q_0) dq_0 + \int_{q_d}^\infty \left[1 - \frac{q_0^r - q_d^r}{arT_d} \right] p_{Q_0}(q_0) dq_0 \tag{A9}$$

Inserting $p_{Q_0}(q_0) = \frac{\gamma_Q^{1+m}}{\Gamma(m+1)} \exp(-\gamma_Q q_0) q_0^m$, we have:

$$P_{Q_d}(q_d) = 1 + \frac{q_d^r}{arT_d} \frac{\Gamma_U(m+1, \gamma_Q q_d)}{\Gamma(m+1)}$$

$$- \frac{\gamma_Q^{-r}}{arT_d} \frac{\Gamma_U(r+m+1, \gamma_Q q_d)}{\Gamma(m+1)} \tag{A10}$$

However, if $r > 0$ or $q_d \leq (-arT_d)^{1/r}$, all three regions exist and equation (A1) integrates as:

$$P_{Q_d}(q_d) = P\{Q_d \leq q_d\} = \int_0^\infty P_{Q_d|Q_0}(q_d, q_0) p_{Q_0}(q_0) dq_0$$

$$= \int_0^{q_d} 1 \cdot p_{Q_0}(q_0) dq_0 + \int_{q_0, T_d}^\infty 0 \cdot p_{Q_0}(q_0) dq_0$$

$$+ \int_{q_d}^{q_0, T_d} \left[1 - \frac{q_0^r - q_d^r}{arT_d} \right] p_{Q_0}(q_0) dq_0 \tag{A11}$$

The bound q_{0, T_d} is obtained by solving equation (A2) for q_0 at $t = T_d$:

$$q_{0, T_d} = (q_d^r + arT_d)^{1/r} \tag{A12}$$

Inserting $p_{Q_0}(q_0) = \frac{\gamma_Q^{1+m}}{\Gamma(m+1)} \exp(-\gamma_Q q_0) q_0^m$ we have:

3. In the third region streamflow takes the value of q_d at some point during the dry season. This case occurs for all values of q_0 that are excluded from the two other regions. The related conditional probability can be obtained by inverting equation (A2):

$$P_{Q_d|Q_0}(q_d, q_0) = 1 - \frac{q_0^r - q_d^r}{arT_d} \tag{A8}$$

The boundaries of these three regions are combined for $r > 0$ and $r < 0$ to obtain the CDF of dry season streamflow conditional on Q_0 described in equation (12).

A2. Integration of the Unconditional Streamflow CDF

Knowing the distribution of Q_0 , we apply the law of total probabilities to derive the unconditional streamflow CDF. In order to do so, we integrate equation (A1) within

the bounds of the 3 regions described above. If $r < 0$ and $q_d > (-arT_d)^{1/r}$, the second region does not exist

and equation (A1) integrates as:

the bounds of the 3 regions described above. If $r < 0$ and $q_d > (-arT_d)^{1/r}$, the second region does not exist

and equation (A1) integrates as:

the bounds of the 3 regions described above. If $r < 0$ and $q_d > (-arT_d)^{1/r}$, the second region does not exist

and equation (A1) integrates as:

the bounds of the 3 regions described above. If $r < 0$ and $q_d > (-arT_d)^{1/r}$, the second region does not exist

and equation (A1) integrates as:

the bounds of the 3 regions described above. If $r < 0$ and $q_d > (-arT_d)^{1/r}$, the second region does not exist

and equation (A1) integrates as:

the bounds of the 3 regions described above. If $r < 0$ and $q_d > (-arT_d)^{1/r}$, the second region does not exist

and equation (A1) integrates as:

the bounds of the 3 regions described above. If $r < 0$ and $q_d > (-arT_d)^{1/r}$, the second region does not exist

and equation (A1) integrates as:

the bounds of the 3 regions described above. If $r < 0$ and $q_d > (-arT_d)^{1/r}$, the second region does not exist

and equation (A1) integrates as:

the bounds of the 3 regions described above. If $r < 0$ and $q_d > (-arT_d)^{1/r}$, the second region does not exist

and equation (A1) integrates as:

the bounds of the 3 regions described above. If $r < 0$ and $q_d > (-arT_d)^{1/r}$, the second region does not exist

and equation (A1) integrates as:

the bounds of the 3 regions described above. If $r < 0$ and $q_d > (-arT_d)^{1/r}$, the second region does not exist

and equation (A1) integrates as:

the bounds of the 3 regions described above. If $r < 0$ and $q_d > (-arT_d)^{1/r}$, the second region does not exist

and equation (A1) integrates as:

the bounds of the 3 regions described above. If $r < 0$ and $q_d > (-arT_d)^{1/r}$, the second region does not exist

and equation (A1) integrates as:

the bounds of the 3 regions described above. If $r < 0$ and $q_d > (-arT_d)^{1/r}$, the second region does not exist

and equation (A1) integrates as:

the bounds of the 3 regions described above. If $r < 0$ and $q_d > (-arT_d)^{1/r}$, the second region does not exist

and equation (A1) integrates as:

the bounds of the 3 regions described above. If $r < 0$ and $q_d > (-arT_d)^{1/r}$, the second region does not exist

and equation (A1) integrates as:

the bounds of the 3 regions described above. If $r < 0$ and $q_d > (-arT_d)^{1/r}$, the second region does not exist

and equation (A1) integrates as:

the bounds of the 3 regions described above. If $r < 0$ and $q_d > (-arT_d)^{1/r}$, the second region does not exist

and equation (A1) integrates as:

the bounds of the 3 regions described above. If $r < 0$ and $q_d > (-arT_d)^{1/r}$, the second region does not exist

and equation (A1) integrates as:

the bounds of the 3 regions described above. If $r < 0$ and $q_d > (-arT_d)^{1/r}$, the second region does not exist

and equation (A1) integrates as:

$$\begin{aligned}
 P_{Q_d}(q_d) &= 1 + \frac{q_d^r}{arT_d} \frac{\Gamma_U(m+1, \gamma_Q q_d)}{\Gamma(m+1)} \\
 &\quad - \left(1 + \frac{q_d^r}{arT_d} \right) \frac{\Gamma_U(m+1, \gamma_Q (q_d^r + arT_d)^{1/r})}{\Gamma(m+1)} \\
 &\quad + \frac{\gamma_Q^{-r}}{arT_d} \frac{\Gamma_U(r+m+1, \gamma_Q (q_d^r + arT_d)^{1/r})}{\Gamma(m+1)} \\
 &\quad - \frac{\gamma_Q^{-r}}{arT_d} \frac{\Gamma_U(r+m+1, \gamma_Q q_d)}{\Gamma(m+1)}
 \end{aligned} \tag{A13}$$

Combining equations (A10) and (A13) and their respective domains, we finally obtain the expression for the CDF of dry season streamflow described in equation (13).

Acknowledgments

The authors would like to thank Michèle Müller for her invaluable assistance in analytical derivation, and A. Castellarin and three anonymous reviewers for their helpful review and comments. Data have been graciously provided by the Department of Hydrology and Meteorology of Nepal, the HKH-FRIEND project, the US Geological Survey, the California Irrigation Management Information System, the Western Australian Department of Water, and the Australian Bureau of Meteorology. Gopal Penny and Artemis Kitsios are gratefully acknowledged for the photographs. The Fulbright Science and Technology Fellowship and the Swiss National Science Foundation are gratefully acknowledged for funding (M.F.M.). S.T. acknowledges support from NSF EAR-1331940.

References

- Acreman, M., and M. J. Dunbar (1999), Defining environmental river flow requirements—A review, *Hydrol. Earth Syst. Sci.*, 8(5), 861–876, doi:10.5194/hess-8-861-2004.
- Alaouze, C. M. (1989), Reservoir releases to uses with different reliability requirements, *Water Resour. Bull.*, 25(6), 1163–1168, doi:10.1111/j.1752-1688.1989.tb01328.x.
- Andermann, C., L. Longuevergne, S. Bonnet, A. Crave, P. Davy, and R. Gloaguen (2012), Impact of transient groundwater storage on the discharge of Himalayan rivers, *Nat. Geosci.*, 5(2), 127–132, doi:10.1038/ngeo1356.
- Barron, O., M. Donn, S. Furby, J. Chia, and C. Johnstone (2009), Groundwater contribution to nutrient export from the Ellenbrook catchment, *Water for a Healthy Country Flagship Rep. Ser.*, EP116498 Commonw. Sci. and Ind. Res. Organ, Clayton South, Australia.
- Basso, S., and G. Botter (2012), Streamflow variability and optimal capacity of run-of-river hydropower plants, *Water Resour. Res.*, 48, W10527, doi:10.1029/2012WR012017.
- Basu, N. B., P. S. C. Rao, S. E. Thompson, N. V. Loukinova, S. D. Donner, S. Ye, and M. Sivapalan (2011), Spatiotemporal averaging of in-stream solute removal dynamics, *Water Resour. Res.*, 47, W00J06, doi:10.1029/2010WR010196.
- Bélisle, C. J. (1992), Convergence theorems for a class of simulated annealing algorithms on Rd, *J. Appl. Probab.*, 29(4), 885–895.
- Botter, G., A. Porporato, I. Rodriguez-Iturbe, and A. Rinaldo (2007a), Basin-scale soil moisture dynamics and the probabilistic characterization of carrier hydrologic flows: Slow, leaching-prone components of the hydrologic response, *Water Resour. Res.*, 43, W02417, doi:10.1029/2006WR005043.
- Botter, G., F. Peratoner, A. Porporato, I. Rodriguez-Iturbe, and A. Rinaldo (2007b), Signatures of large-scale soil moisture dynamics on streamflow statistics across US climate regimes, *Water Resour. Res.*, 43, W11413, doi:10.1029/2007WR006162.
- Botter, G., S. Zanardo, A. Porporato, I. Rodriguez-Iturbe, and A. Rinaldo (2008), Ecohydrological model of flow duration curves and annual minima, *Water Resour. Res.*, 44, W08418, doi:10.1029/2008WR006814.
- Botter, G., A. Porporato, I. Rodriguez-Iturbe, and A. Rinaldo (2009), Nonlinear storage-discharge relations and catchment streamflow regimes, *Water Resour. Res.*, 45, W10427, doi:10.1029/2008WR007658.
- Botter, G., S. Basso, I. Rodriguez-Iturbe, and A. Rinaldo (2013), Resilience of river flow regimes, *Proc. Natl. Acad. Sci. U. S. A.*, 110(32), 12,925–12,930.
- Brutsaert, W., and J. L. Nieber (1977), Regionalized drought flow hydrographs from a mature glaciated plateau, *Water Resour. Res.*, 13(3), 637–643, doi:10.1029/WR013i003p00637.
- Bureau of Meteorology (2013), *Climate Data Online*, Gov. of Aust.
- California Irrigation Management Information System (2013), *Daily Rainfall Data*, Dep. of Water Resour.
- Castellarin, A., R. Vogel, and A. Brath (2004a), A stochastic index flow model of flow duration curves, *Water Resour. Res.*, 40, W03104, doi:10.1029/2003WR002524.
- Castellarin, A., G. Galeati, L. Brandimarte, A. Montanari, and A. Brath (2004b), Regional flow-duration curves: Reliability for ungauged basins, *Adv. Water Resour.*, 27(10), 953–965, doi:10.1016/j.advwatres.2004.08.005.
- Castellarin, A., G. Camorani, and A. Brath (2007), Predicting annual and long-term flow-duration curves in ungauged basins, *Adv. Water Resour.*, 30(4), 937–953, doi:10.1016/j.advwatres.2006.08.006.
- Castellarin, A., et al. (2013), Prediction of flow duration curves in ungauged basins, in *Runoff Prediction in Ungauged Basins: Synthesis across Processes, Places and Scales*, edited by G. Blöchl et al., chap. 7, pp. 135–162, Cambridge Univ. Press, Cambridge, U. K.
- Ceola, S., G. Botter, E. Bertuzzo, A. Porporato, I. Rodriguez-Iturbe, and A. Rinaldo (2010), Comparative study of ecohydrological streamflow probability distributions, *Water Resour. Res.*, 46, W09502, doi:10.1029/2010WR009102.
- Chalise, S., S. Kansakar, G. Rees, K. Croker, and M. Zaidman (2003), Management of water resources and low flow estimation for the Himalayan basins of Nepal, *J. Hydrol.*, 282(1–4), 25–35.
- Cheng, L., M. Yaeger, A. Viglione, E. Coopersmith, S. Ye, and M. Sivapalan (2012), Exploring the physical controls of regional patterns of flow duration curves. Part 1: Insights from statistical analyses, *Hydrol. Earth Syst. Sci.*, 16, 4435–4446, doi:10.5194/hess-16-4435-2012.
- Chow, V. T. (1964), *Handbook of Applied Hydrology: A Compendium of Water-Resources Technology*, McGraw-Hill, N. Y.
- CIESIN (2012), *National Aggregates of Geospatial Data Collection: Population, Landscape, And Climate Estimates, Version 3 (PLACE III)*, NASA Socioecon. Data and Appl. Cent., N. Y.
- Coopersmith, E., M. Yaeger, S. Ye, L. Cheng, and M. Sivapalan (2012), Exploring the physical controls of regional patterns of flow duration curves—Part 3: A catchment classification system based on regime curve indicators, *Hydrol. Earth Syst. Sci.*, 16, 4467–4482, doi:10.5194/hess-16-4467-2012.
- Department of Hydrology and Meteorology (2011), *Daily Streamflow and Precipitation Data*, Ministry of Science, Technology and Environment, Kathmandu, Nepal.
- Department of Water (2013), *Hydstra Database*, Water Inf. Provision Sect., Perth, West. Aust.
- Dominguez, F., E. Rivera, D. Lettenmaier, and C. Castro (2012), Changes in winter precipitation extremes for the Western United States under a warmer climate as simulated by regional climate models, *Geophys. Res. Lett.*, 39, L05803, doi:10.1029/2011GL050762.

- Fatichi, S., V. Y. Ivanov, and E. Caporali (2012), Investigating interannual variability of precipitation at the global scale: Is there a connection with seasonality?, *J. Clim.*, *25*(16), 5512–5523, doi:10.1175/JCLI-D-11-00356.1.
- García-Ruiz, J. M., J. I. López-Moreno, S. M. Vicente-Serrano, T. Lasanta-Martínez, and S. Beguería (2011), Mediterranean water resources in a global change scenario, *Earth Sci. Rev.*, *105*(3), 121–139, doi:10.1016/j.earscirev.2011.01.006.
- HKH-FRIEND (2004), *Hindu Kush Himalayan—Flow Regimes From International Experimental and Network Data*, UNESCO Int. Hydrol. Programme, Paris, France.
- Hosseini, S., F. Forouzbakhsh, and M. Rahimpoor (2005), Determination of the optimal installation capacity of small hydro-power plants through the use of technical, economic and reliability indices, *Energy Policy*, *33*(15), 1948–1956, doi:10.1016/j.enpol.2004.03.007.
- Jothityangkoon, C., and M. Sivapalan (2001), Temporal scales of rainfall–runoff processes and spatial scaling of flood peaks: Space–time connection through catchment water balance, *Adv. Water Resour.*, *24*(9), 1015–1036, doi:10.1016/S0309-1708(01)00044-6.
- Katz, R., and M. Parlange (1996), Mixtures of stochastic processes: Application to statistical downscaling, *Clim. Res.*, *7*(2), 185–193, doi:10.3354/cr007185.
- Kirchner, J. W. (2009), Catchments as simple dynamical systems: Catchment characterization, rainfall–runoff modeling, and doing hydrology backward, *Water Resour. Res.*, *45*, W02429, doi:10.1029/2008WR006912.
- Kusre, B., D. Baruah, P. Bordoloi, and S. Patra (2010), Assessment of hydropower potential using GIS and hydrological modeling technique in Kopili River basin in Assam (India), *Appl. Energy*, *87*(1), 298–309, doi:10.1016/j.apenergy.2009.07.019.
- Larentis, D., W. Collischonn, F. Olivera, and C. Tucci (2010), GIS-based procedures for hydropower potential spotting, *Energy*, *35*(10), 4237–4243, doi:10.1016/j.energy.2010.07.014.
- Lee, R., J. Brizzee, S. Cherry, and D. Hall (2008), Virtual hydropower prospecting: A foundation for water energy resource planning and development, *J. Map Geogr. Libraries*, *4*(2), 336–347, doi:10.1080/15420350802142678.
- Müller, M. F., and S. E. Thompson (2013), Bias adjustment of satellite rainfall data through stochastic modeling: Methods development and application to Nepal, *Adv. Water Resour.*, *60*, 121–134, doi:10.1016/j.advwatres.2013.08.004.
- Muneepeerakul, R., A. Rinaldo, and I. Rodriguez-Iturbe (2007), Effects of river flow scaling properties on riparian width and vegetation biomass, *Water Resour. Res.*, *43*, W12406, doi:10.1029/2007WR006100.
- Nathan, R., and T. McMahon (1990), Evaluation of automated techniques for base flow and recession analyses, *Water Resour. Res.*, *26*(7), 1465–1473, doi:10.1029/WR026i007p01465.
- Porporato, A., E. Daly, and I. Rodriguez-Iturbe (2004), Soil water balance and ecosystem response to climate change, *Am. Nat.*, *164*(5), 625–632, doi:10.1086/424970.
- Pugliese, A., A. Castellarin, and A. Brath (2013), Geostatistical prediction of flow-duration curves, *Hydrol. Earth Syst. Sci. Discuss.*, *10*, pp. 13053–13091.
- Pumo, D., L. V. Noto, and F. Viola (2013), Ecohydrological modelling of flow duration curve in Mediterranean river basins, *Adv. Water Resour.*, *52*, 314–327, doi:10.1016/j.advwatres.2012.05.010.
- Rianna, M., A. Efstratiadis, F. Russo, F. Napolitano, and D. Koutsoyiannis (2013), A stochastic index method for calculating annual flow duration curves in intermittent rivers, *Irrig. Drain.*, *62*(S2), 41–49.
- Richter, B., J. Baumgartner, R. Wigington, and D. Braun (1997), How much water does a river need?, *Freshwater Biol.*, *37*(1), 231–249, doi:10.1046/j.1365-2427.1997.00153.x.
- Richter, B. D., R. Mathews, D. L. Harrison, and R. Wigington (2003), Ecologically sustainable water management: Managing river flows for ecological integrity, *Ecol. Appl.*, *13*(1), 206–224, doi:10.1890/1051-0761(2003)013[0206:ESWMMR]2.0.CO;2.
- Rodriguez Iturbe, I., and A. Porporato (2004), *Ecohydrology of Water-Controlled Ecosystems: Soil Moisture and Plant Dynamics*, Cambridge Univ. Press, Cambridge, U. K.
- Samuel, J. M., M. Sivapalan, and I. Struthers (2008), Diagnostic analysis of water balance variability: A comparative modeling study of catchments in Perth, Newcastle, and Darwin, Australia, *Water Resour. Res.*, *44*, W06403, doi:10.1029/2007WR006694.
- Santolin, A., G. Cavazzini, G. Pavesi, G. Ardizzon, and A. Rossetti (2011), Techno-economical method for the capacity sizing of a small hydro-power plant, *Energy Convers. Manage.*, *52*(7), 2533–2541, doi:10.1016/j.enconman.2011.01.001.
- Schaeffli, B., A. Rinaldo, and G. Botter (2013), Analytic probability distributions for snow-dominated streamflow, *Water Resour. Res.*, *49*, 2701–2713, doi:10.1002/wrcr.20234.
- Searcy, J. K. (1959), Flow-duration curves manual of hydrology part 2, low-flow techniques: Methods and practices of the geological survey, *U.S. Geol. Surv. Water Supply Pap 1542-A*, pp. 1–33.
- Soetaert, K., T. Petzoldt, and R. W. Setzer (2010), Solving differential equations in R: Package desolve, *J. Stat. Software*, *33*(9), 1–25.
- Sornette, D. (2004), *Critical Phenomena in Natural Sciences*, 2nd ed., Springer, N. Y.
- Stoelzle, M., K. Stahl, and M. Weiler (2013), Are streamflow recession characteristics really characteristic?, *Hydrol. Earth Syst. Sci.*, *17*(2), 817–828, doi:10.5194/hessd-9-10563-2012.
- Tallaksen, L. (1995), A review of baseflow recession analysis, *J. Hydrol.*, *165*(1), 349–370, doi:10.1016/0022-1694(94)02540-R.
- Thompson, S., M. Sivapalan, C. Harman, V. Srinivasan, M. Hipsey, P. Reed, A. Montanari, and G. Blöschl (2013a), Developing predictive insight into changing water systems: Use-inspired hydrologic science for the Anthropocene, *Hydrol. Earth Syst. Sci. Discuss.*, *10*, 7897–7961, doi:10.5194/hessd-10-7897-2013.
- Thompson, S., S. Levin, and I. Rodriguez-Iturbe (2013b), Linking plant disease risk and precipitation drivers: A dynamical systems framework, *Am. Nat.*, *181*(1), E1–E16, doi:10.1086/668572.
- United States Geological Survey (2013), *National Water Information System*, Reston, VA.
- Vogel, R., and N. Fennessey (1994), Flow-duration curves. I: New interpretation and confidence intervals, *J. Water Resour. Plann. Manage.*, *120*(4), 485–504, doi:10.1061/(ASCE)0733-9496(1994)120:4(485).
- Vogel, R. M., and N. M. Fennessey (1995), Flow duration curves II: A review of applications in water resources planning, *Water Resour. Bull.*, *31*(6), 1029–1039, doi:10.1111/j.1752-1688.1995.tb03419.x.
- Ye, S., M. Yaeger, E. Coopersmith, L. Cheng, and M. Sivapalan (2012), Exploring the physical controls of regional patterns of flow duration curves—Part 2: Role of seasonality, the regime curve, and associated process controls, *Hydrol. Earth Syst. Sci.*, *16*, 4447–4465, doi:10.5194/hess-16-4447-2012.
- Yi, C., J. Lee, and M. Shim (2010), Site location analysis for small hydropower using geo-spatial information system, *Renewable Energy*, *35*(4), 852–861, doi:10.1016/j.renene.2009.08.003.